

# Failure of evaporator tubes initiated by lamellar tearing during the commissioning of a waste heat recovery boiler

S. Srikanth <sup>a,\*</sup>, S.K. Das <sup>b</sup>, C. Sasikumar <sup>a</sup>, B. Ravikumar <sup>b</sup>

<sup>a</sup> National Metallurgical Laboratory Chennai Centre, CSIR Madras Complex, Post TTTI, Taramani, Chennai 600 113, India

<sup>b</sup> Materials Science and Technology Division, National Metallurgical Laboratory, Jamshedpur 831 007, India

Received 18 March 2005; accepted 6 April 2005

Available online 31 March 2006

---

## Abstract

Successive failures of several new evaporator tubes during commissioning and trial run of a waste heat recovery boiler has been analyzed. The evaporator tubes are cold bent into U-shape and subsequently TIG welded to a 24-mm thick wear plate on either sides of the tube immediately adjacent to the bend. The failed samples showed stepped longitudinal cracks along the rolling direction and parallel to the weld fusion boundary at the fireside surface of the inner bend of the tube, prominently at the center of the bend. It was found that the failure of the evaporator tubes at the tube bends was initiated by lamellar tearing because of inherent defects in the material (segregation leading to banded structure), improper processing of material (inclusions with high aspect ratios along the rolling direction) and accelerated by high transverse shrinkage stresses over the entire bend portion of the tube introduced by the weld. The pre-existing fine cracks in the welded evaporator tube initiated by lamellar tearing have subsequently opened up during service when the total strain in the region increased because of steam pressure resulting in catastrophic failure of the tubes. Contrary to expectation, many of the elongated inclusions were found to be iron oxide scales and only few were manganese sulfide stringers enveloped by iron oxide scales. The iron oxide inclusions were resolved from the manganese sulfide by scanning electron microscopy and EDS spot analysis of the inclusions.

© 2006 Elsevier Ltd. All rights reserved.

**Keywords:** Lamellar tearing; Manganese sulfide stringers; Iron oxide scales

---

## 1. Background

Catastrophic failure in about 23 tube bends in the evaporators within 15 days of commencing the trial runs in the boiler was reported in an 8.5 MW waste heat recovery boiler. During the trial runs, light diesel oil was being used as fuel.

The evaporator tubes (38.2 mm OD, 4 mm thick) are cold bent into U shape with an inner radius of 50 mm. The bends are subsequently TIG welded (double sided fillet welds of size 3 mm each) to a 24 mm thick wear

---

\* Corresponding author. Tel.: +91 44 2254 2077; fax: +91 44 2254 1027.

E-mail address: [s\\_srikanth\\_99@yahoo.com](mailto:s_srikanth_99@yahoo.com) (S. Srikanth).

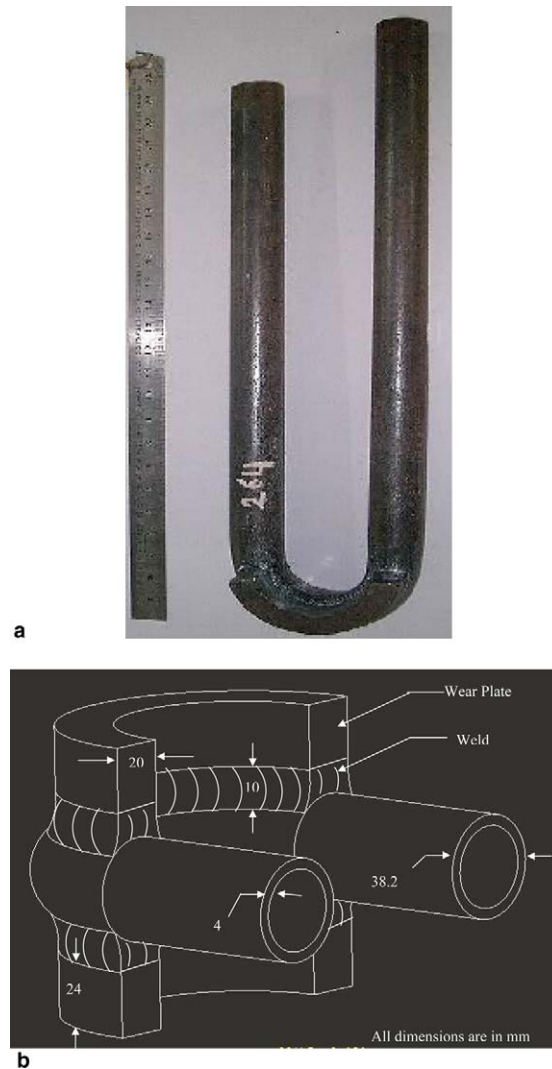


Fig. 1. Section of the evaporator tube showing the wear plate welded at the bend.

plate made of ASTM-A387 on either sides of the tube at the bend. The weld joint is similar to that of a T-joint. The length of the weld or the fusion zone on either side of the bend in each tube is 116 mm. The tube bends as well as the welds were reported to be routinely subjected to dye penetrant test and the coils to a pneumatic test at  $0.5 \text{ kg/cm}^2$  and a hydrostatic test at  $75 \text{ kg/cm}^2$ . All the evaporator tubes commissioned in the boiler are reported to have passed the tests. The evaporator tubes are not subjected to stress relieving after bending as well as after welding to the wear plates. The evaporator tubes are seamless and were reported to conform to the chemical and mechanical requirements of ASTM-A210 Grade A1, prior to bending of tube and welding of wear plate. A photograph of the evaporator tube along with the wear plate welded at the bend is depicted in Fig. 1. Three of the failed evaporator tubes (F1, F2 and F3) as well as two unused evaporator tubes (UF1 and UF2) were taken up for a thorough investigation.

## 2. Experimental

The failed surfaces and samples (horizontal and the bend portions) cut from the failed as well as the unused tubes were subjected to visual and macro examination, chemical analysis, X-ray radiography, fractography, microscopic examination (under unetched and etched conditions) at various locations, mechanical property

measurements and EDS analysis using SEM. Further, polished samples from the unused evaporator tube were also examined in the SEM for morphological features. Chemical analyses were carried out in an Optical Emission Spectrophotometer (Spectrolab Germany), macroscopic examination in a stereomicroscope (Leica, Switzerland), microscopic examination in an optical microscope (LEICA DMLM, Switzerland) and a Scanning Electron Microscope with EDS attachment (Jeol JSM 840A), hardness measurements in a Vickers hardness tester (Indentec, UK) and a LEICA VMHT microhardness tester. Real-time X-ray radiographic measurements were carried out in a 225 KVA radiographic tester (Siefert, Germany) that has a resolution of 1.5% of the thickness of the sample and mechanical property measurements (tensile and yield strength, elongation, flattening test and drift expansion test) using standard methods. The tensile and flattening tests were carried out according to ASTM A370 and the drift expansion test as per IS 2335. For one of the failed tube samples and an unused evaporator tube sample, the residual stress was also measured on the fireside surface of the outer bend by X-ray diffraction method.

### 3. Results

#### 3.1. Failed tube samples

Almost all the failed tube samples showed visible longitudinal cracks along the rolling direction at the fireside surface of the inner bend of the tube and prominently at the center of the bend. Stereomicroscopic pictures of the centerline cracks observed at the fireside surface of inner bends in three of the failed samples are depicted in Fig. 2. The X-ray radiographs of two of these samples are also shown in Fig. 3. Fine visible cracks were also observed in the waterside surfaces of the failed samples, especially near the weld. The stereo-micrographs of the waterside surface depicting the cracks are shown in Fig. 4. The failed samples also showed transverse cracks when observed at higher magnifications as shown in Fig. 5(a). The micrographs in the unetched condition of the failed samples showed several sulfide type inclusions with high aspect ratios and elongated along the rolling direction as shown in Fig. 5(b and c). The elongated inclusions could be either manganese sulfide or iron oxide inclusions. It is difficult to distinguish them in optical microscopy. Both, manganese sulfide and iron oxide inclusions appear light gray in vertical bright-field illumination and both are plastic (i.e., easily deformed) at lower temperatures. Attempts to resolve them in optical microscopy by using special etching techniques [1,2] were unsuccessful. Some globular oxide type inclusions are also evident in these micrographs. Fine cracks interconnecting the elongated inclusions, both in the longitudinal and transverse directions are observed in these unetched micrographs. The microstructures (observed after etching) of samples drawn from various locations in the bend region of the failed tubes are illustrated in Fig. 6(a–f). There are several striking features observed in the micrographs. All the samples, except those very close to the weld show a banded ferrite and pearlite structure, the banding being along the rolling direction. There were several inclusions with high aspect ratios, elongated along the longitudinal direction and located preferentially within the ferrite bands (Figs. 6a and d). At higher magnifications, the interconnection of the elongated inclusions through fine cracks is also obvious (Fig. 6c). However, fine cracks connecting groups of inclusions in the transverse direction could also be seen (Fig. 6e). The microstructures very close to the weld region show the formation of bainite as seen in Fig. 6(f). The SEM fractograph of one of the failed tubes is depicted in Fig. 7. The fractographs of all the failed samples show extensive iron oxide rust covering the fracture surface. Mild cleaning of the fracture surface with dilute acids could not remove the iron oxide from the fracture surface. Although the fractographs of the failed samples were not very clear because of the iron oxide coating at the fracture surface, features characteristic of a brittle transgranular fracture could be distinguished. In some of the fractographs, a stepped appearance of the fracture surface could also be distinguished. The elemental analysis of the fracture surface by energy dispersive spectral (EDS) analysis (Fig. 7b) shows the presence of only Fe, Mn, Si and traces of Ca. Bulk elemental analysis using EDS are only approximate and should be cross-checked against direct conventional/instrumental analysis.

The chemical analysis of one of the failed samples is given in Table 1 in comparison to the requirements of ASTM-A210 Gr.A1. It was observed that the chemical composition of all the failed samples not only conform to the requirements of the standard, but also show low levels of sulfur and phosphorus

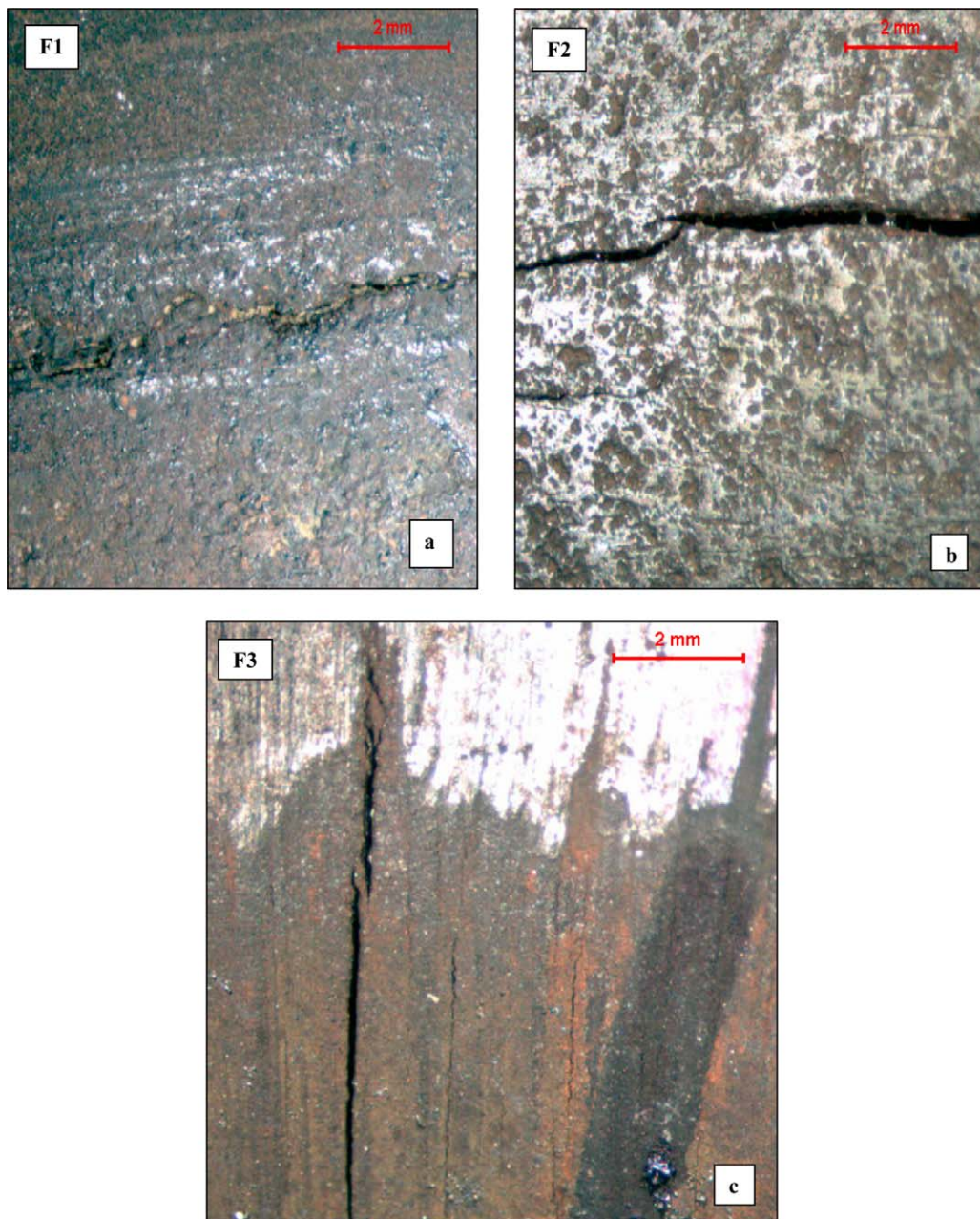


Fig. 2. Stereo images showing longitudinal cracks in the fireside surface of the inner bend (at the centre) of the failed tubes F1, F2 and F3, respectively.

(0.005–0.007%). The results of the mechanical tests on the samples cut out from the horizontal section of one of the failed tubes are summarized in Table 2 in comparison to the requirements of the standard. It was found that although the tensile and yield strengths are much above the requirements of ASTM-A210 Gr.A1, the ductility (% elongation) is somewhat lower than the specified value. Further, it was observed that all the failed tubes did not pass the drift expansion test. The samples subject to drift expansion test showed cracks along the rolling direction especially on the waterside surface. The chemical composition as well as the mechanical properties of all the failed samples was similar. The micro-hardness results along

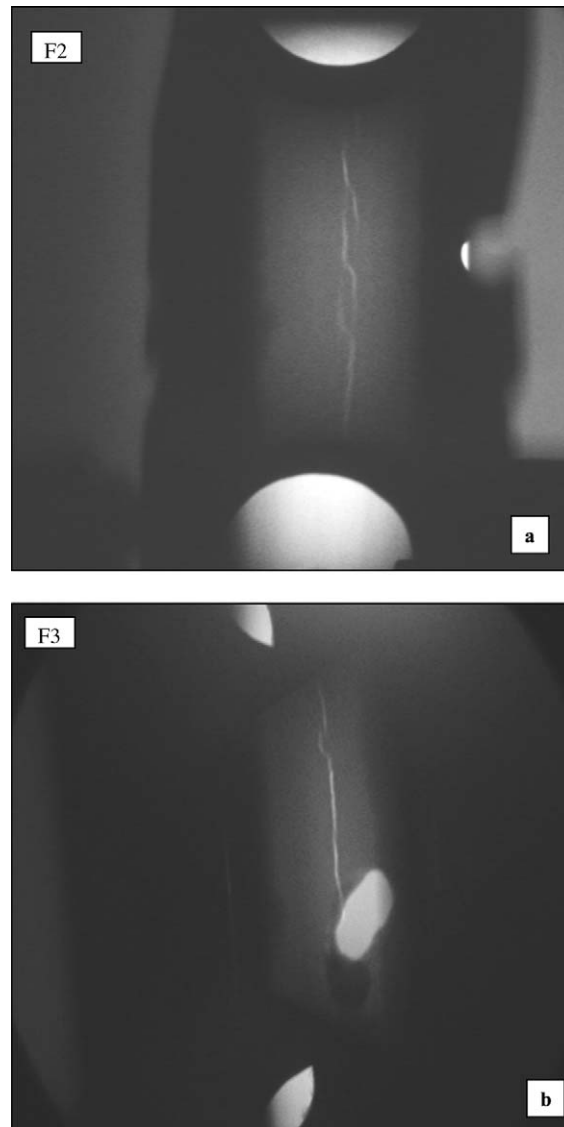


Fig. 3. X-ray radiographs of failed bend tube samples F2 and F3 showing long longitudinal cracks along the rolling direction at the center of the bend. The cracks appear stepped with treads parallel to the rolling plane. The large holes appearing in the radiographs (right hand side) are holes punched to drain the water.

the cross-section of the tube at the bend for one of the failed samples is summarized in Table 3. It is seen that the micro-hardness values at the bend region where the tube is welded to the wear plate is extremely high (200–240  $HV_{0.1}$ ) all through the cross-section and specifically at the fireside surface. The micro-hardness values at the bend for the other failed tubes also showed similar high values and the same trend. However, the micro-hardness values at the horizontal section of the tube far away from the bend (welded region) were normal (140–150  $HV_{0.1}$ ). The residual stress values measured at the fireside surface of one of the failed tubes at the bend region are given in Fig. 8. The residual stress values at the outer fireside surface show large values of compressive stresses. During the bending operation, the outer portion of the bend is subjected to tensile plastic strain. Elastic spring-back after bending results in a compressive residual stress on the outside of the bend. Calculations of the residual stress give values close to those observed experimentally. Residual stresses could not be measured at the fireside surface of the inner bend or in the waterside surfaces because of difficulties, associated with the geometry of the sample.



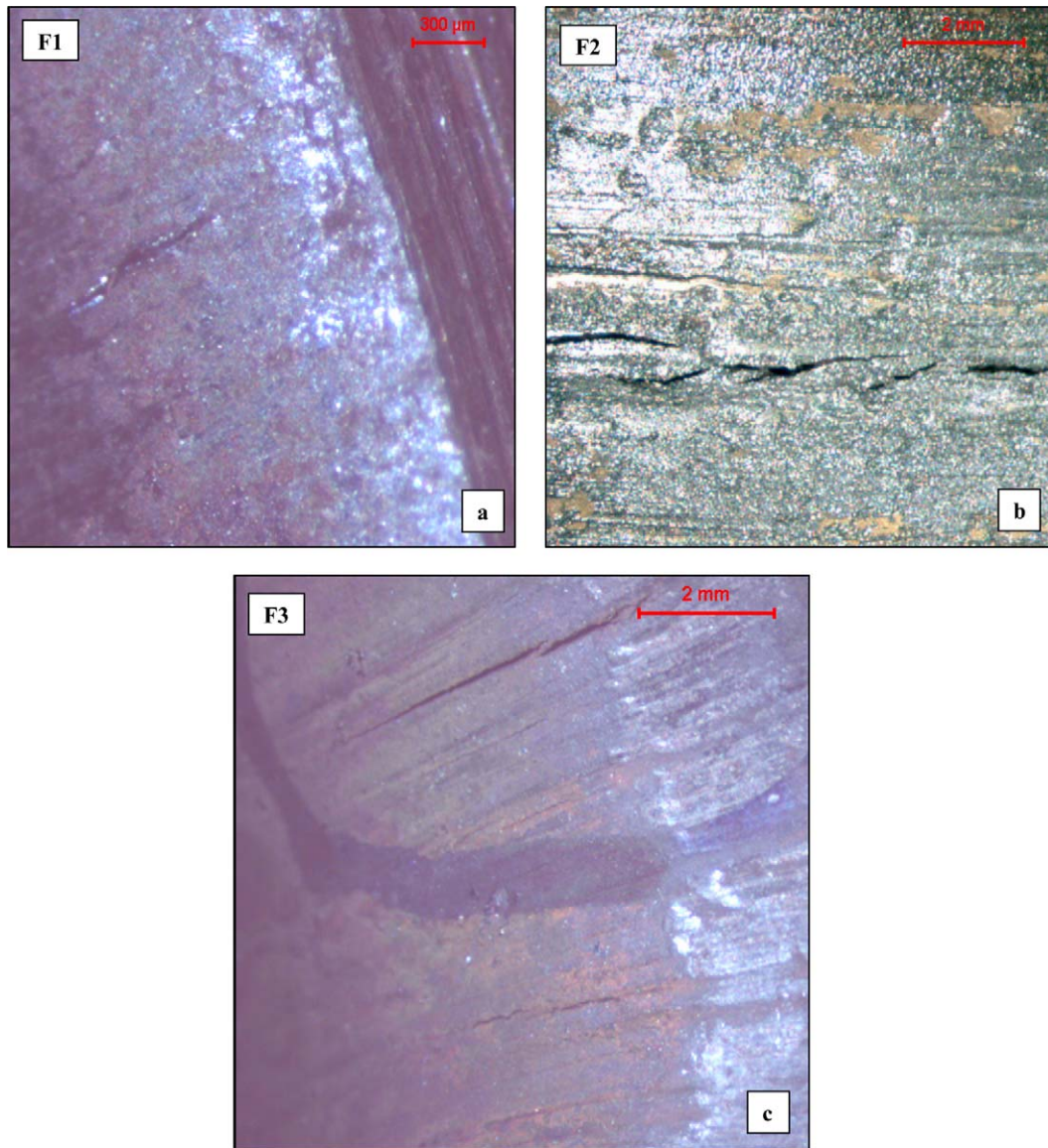


Fig. 4. Stereo images of the waterside surface of the failed samples showing longitudinal cracks along the rolling direction.

### 3.2. Virgin tube samples (welded to the wear plate)

The results of chemical analysis and mechanical property measurements of the virgin tube samples (at the horizontal section) are also summarized in Tables 1 and 2, respectively. The virgin tube samples meet the chemical and mechanical requirements of ASTM-A210 Gr.A1. However, similar to the failed samples, the micro-hardness values at the bend region, where the tube is welded to the wear plate is extremely high (200–240 HV<sub>0.1</sub>) all through the cross-section and specifically at the fireside surface. The residual stress at the outer fireside surface also showed large compressive stresses. Further, the tube also failed the drift expansion test.

The unused tube samples showed elongated inclusions and several fine cracks mainly along the rolling direction when viewed at magnification under a stereomicroscope (Fig. 9). These cracks were prominent at the bend region of the tube, specifically near the weldment. The microstructures in the unetched condition

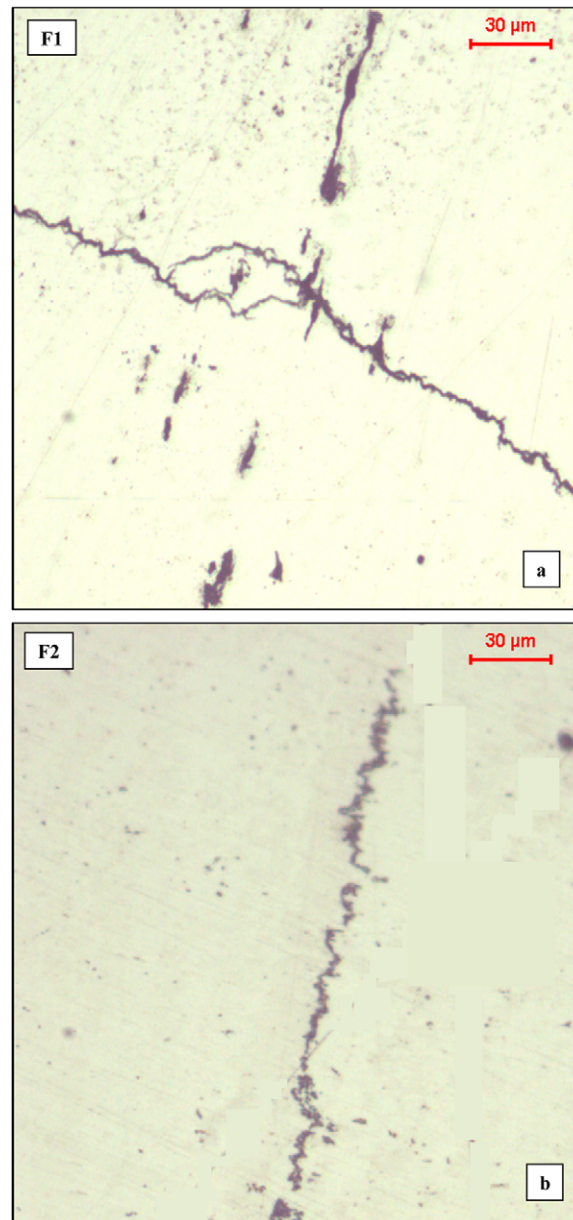


Fig. 5. Micrographs in the unetched condition of samples cut from the waterside surface at the region of failure from two different failed tubes. (a) Continuous crack in the transverse direction of the tube and a large volume fraction of elongated inclusions with high aspect ratios are observed and (b) inclusions elongated in the rolling direction and fine cracks interconnecting the inclusions are seen. Globular oxide type inclusions are also observed.

(Fig. 10) once again clearly showed large volume fraction of long sulfide type inclusions elongated along the rolling direction. These elongated inclusions appear interconnected by fine cracks. Some globular oxide type inclusions were also observed. The microstructures in the etched condition (Fig. 11) once again showed a banded pearlite and ferrite structure along the rolling direction, large volume fraction of inclusions with high aspect ratios, preferential location of the elongated inclusions on the ferrite bands and fine cracks interconnecting the inclusions. The fine transverse cracks that were observed in the failed samples were not present in the virgin tube samples. The results of scanning electron microscopy (secondary electron images) of the polished and etched (2% Nital) samples drawn from the various locations (fireside and waterside surfaces) of this



unused evaporator bend tube are depicted in Fig. 12. It is seen that there are several long elongated inclusions of mostly iron oxide (appearing dark in the SEM secondary electron images) and some manganese sulfide (appearing light gray) in the rolling direction at all locations including the fireside and waterside surfaces. Several longitudinal cracks along the inclusions are also visible. The EDS analysis of the inclusions appearing in dark and light gray contrast is given in Fig. 13. EDS analysis confirm that the inclusions showing a light gray contrast is predominantly manganese sulfide and the iron oxide streaks appear dark.

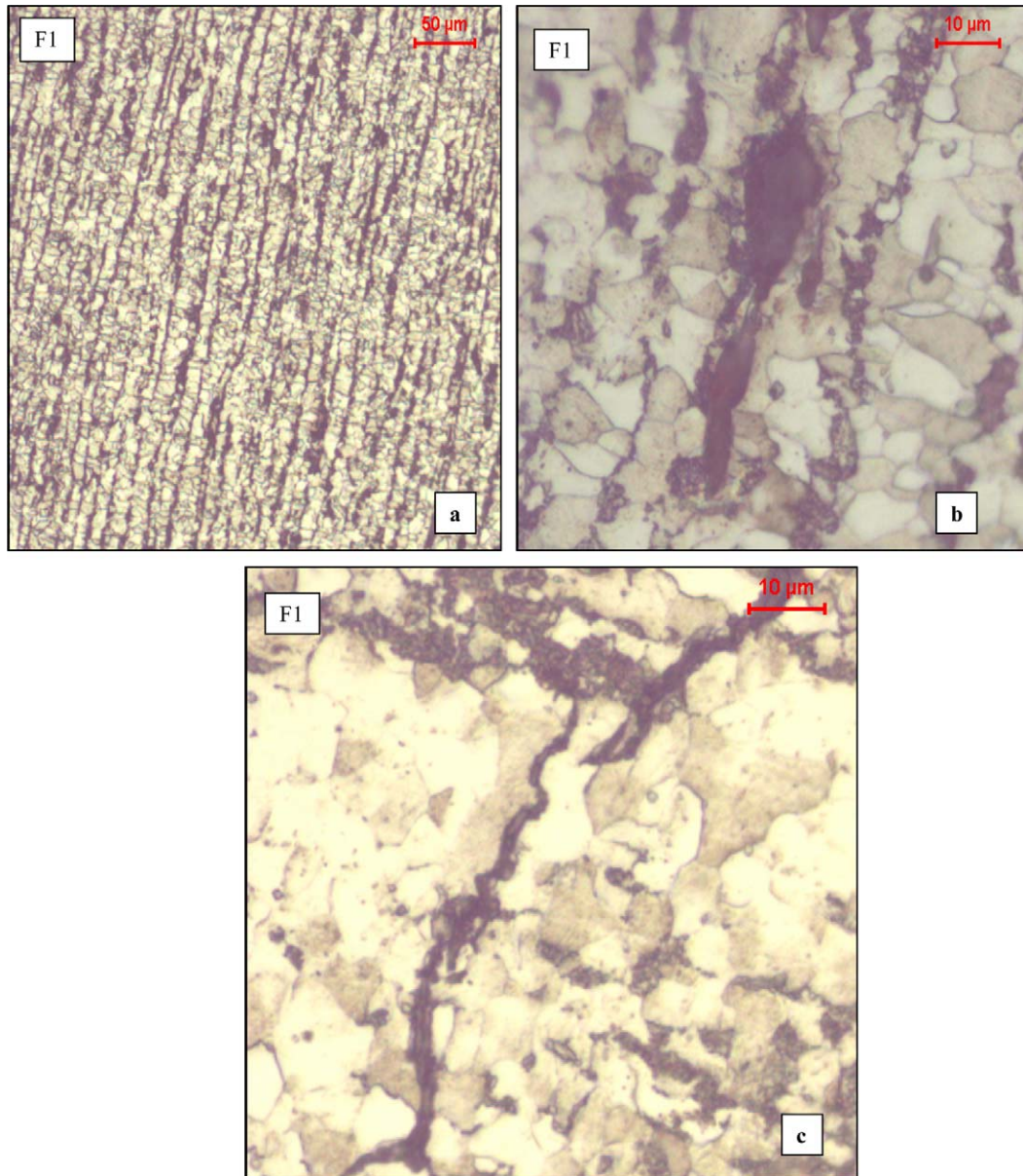


Fig. 6. Micrographs (at different magnification) in etched condition of samples cut from different locations in the failed zone of two different failed tubes: (a) microstructure at the fireside surface of the bend showing polygonal banded ferrite and pearlite; (b) micrograph at higher magnification showing groups of interconnected inclusions; (c) microstructure showing the propagation of crack along the inclusions; (d) microstructure showing a banded structure and elongated inclusions preferentially located within the ferrite bands; (e) microstructure showing fine micro-cracks connecting the groups of inclusions and (f) microstructure of sample from close to the weld region showing the formation of bainite.



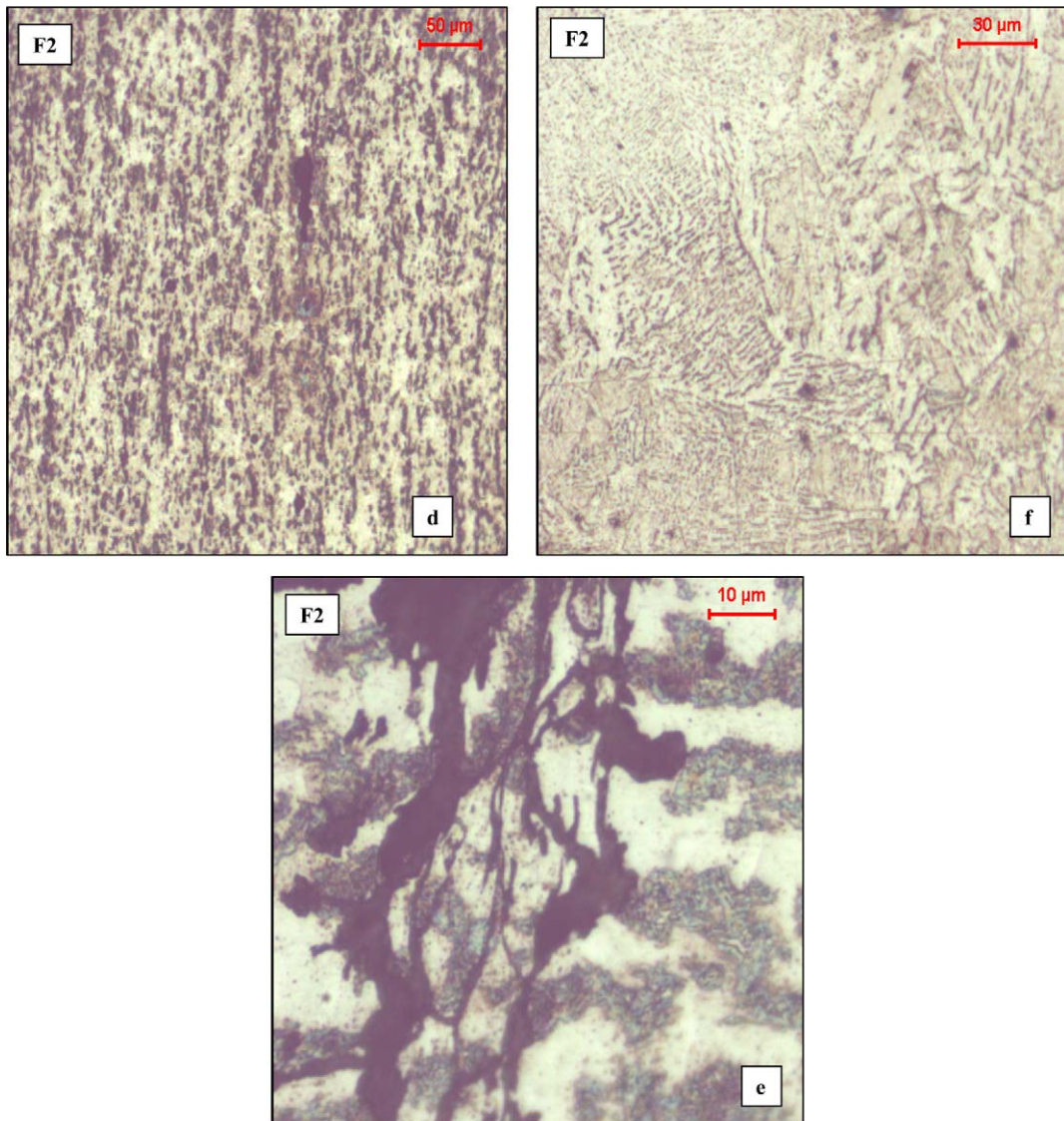


Fig. 6 (continued)

## 4. Discussion

### 4.1. Defects in raw material, virgin tubes and wear plate welded bends

Macroscopic (stereo-images) and microscopic (optical and scanning electron microscopy) analysis of the virgin (unused) evaporator tubes clearly indicate the presence of significant inherent defects, such as elongated inclusions with high aspect ratios, fine cracks along the inclusions in the rolling direction of the material and segregation in the material reflected by the banding of ferrite and pearlite.

#### 4.1.1. Inclusions

The inclusions detected in the virgin tubes, in morphology (ellipsoidal shapes) and appearance (light gray) appear like type I manganese sulfide inclusions in vertical bright-field illumination under an optical microscope. However, since the sulfur content of the steel is less than 0.007%, it is unlikely that the large volume

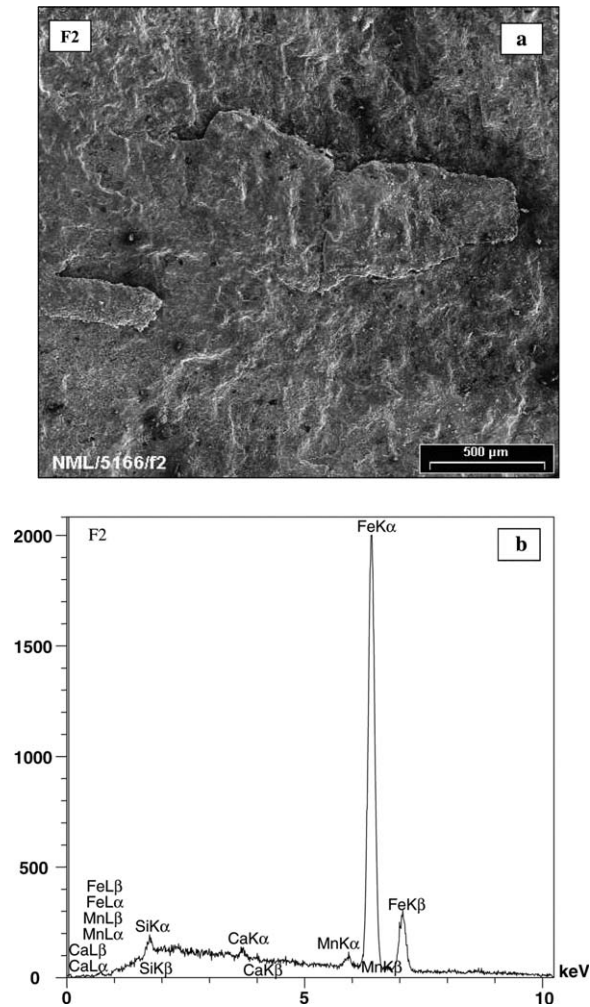


Fig. 7. (a) SEM fractograph of one of the failed surfaces showing extensive iron oxide covering the fracture surface. Features of brittle transgranular fracture observed and (b) EDS elemental analysis of the fracture surface showing only the constituents of steel.

Table 1

Bulk chemical analysis of the failed and virgin tube samples in comparison to the standard (ASTM A213Gr. A1)

Element	Chemical analysis (wt%)		
	Failed tube	Virgin tube	Requirements of ASTM A210 Gr.A1
C	0.18	0.18	0.27 maximum
Si	0.22	0.23	0.10 minimum
Mn	0.85	0.84	0.93 maximum
S	0.006	0.006	0.058 maximum
P	0.006	0.006	0.048 maximum

fraction of the inclusions observed in these samples correspond to MnS alone. It is possible to confuse iron oxide inclusions with MnS inclusions, which also appear light gray and are plastic (i.e., easily deformed) at lower temperatures [3]. Special etching techniques are required to resolve them in optical microscopy [1,2]. Secondary electron imaging in a scanning electron microscope and energy dispersive spectral (EDS) analysis indicated that these elongated inclusions are mainly iron oxide and not manganese sulfide as was originally

Table 2

Bulk mechanical properties of the failed and virgin tube samples (at the horizontal section) in comparison to the standard (ASTM A213Gr. A1)

Mechanical property (at horizontal section of tube)	Failed tube	Virgin tube	Requirements of ASTM A210 Gr.A1
Yield strength	392 MPa	358 MPa	255 MPa minimum
Tensile strength	506 MPa	524 MPa	415 MPa minimum
% elongation	28.3%	30.5 MPa	30% minimum
Hardness	78 HRB	78 HRB	79 HRB maximum
Flattening test	Passes the test	Passes the test	No cracks after test
Drift expansion test	Fails the test	Fails the test	No cracks after test

Table 3

Results of micro-hardness measurements across the tube thickness at the tube bend (after welding of wear plate)

↓ along the longitudinal direction	Micro-hardness (HV <sub>0.1</sub> ) → across the thickness of tube at the bend		
	Waterside surface	Cross-section	Fireside surface
	219	225	236
	222	212	239
	234	217	237
	217	221	239
	219	219	241

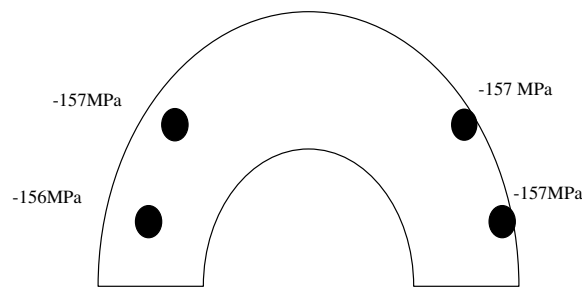


Fig. 8. Residual stresses at the outer fireside surface of the bend in one of the failed tubes.

presumed. Both FeO and (FeMn)O are plastic at room temperature, but gradually become less plastic above 400 °C [4].

Elongated non-metallic inclusions can result in the tubes having a low ductility in the through thickness direction, because of the weak interfacial bond between them and the matrix. The ductility in the transverse direction given by the short transverse reduction in area (STRA) is determined principally by the nature and distribution of the non-metallic inclusions present. Stringers of inclusions that are long and somewhat irregular in shape results in the low STRA values. It has been stipulated [3] that the maximum length of inclusions in the principal plate rolling direction should not exceed about 100 μm. When large numbers of grouped inclusions are present, a more sophisticated measure of permissible inclusion size; the projected inclusion length (i.e., the total projected length of inclusions per unit area of transverse section) is adopted. Maximum permissible values of the projected inclusion length are much lower.

In the present case, the large volume fraction of long iron oxide/MnS inclusions (>100 μm) and the high aspect ratios of these inclusions along the rolling direction in the virgin tubes is likely to decrease the transverse ductility considerably. It is possible that the iron oxide scale on the surface of the material has got rolled in during the hot rolling of the sheets/plates.

#### 4.1.2. Ferrite–pearlite banding

The microstructure of the virgin tubes shows a banded ferrite and pearlite structure in both the longitudinal and transverse sections. The banding occurs because of a longitudinal inhomogeneity that results in preferen-

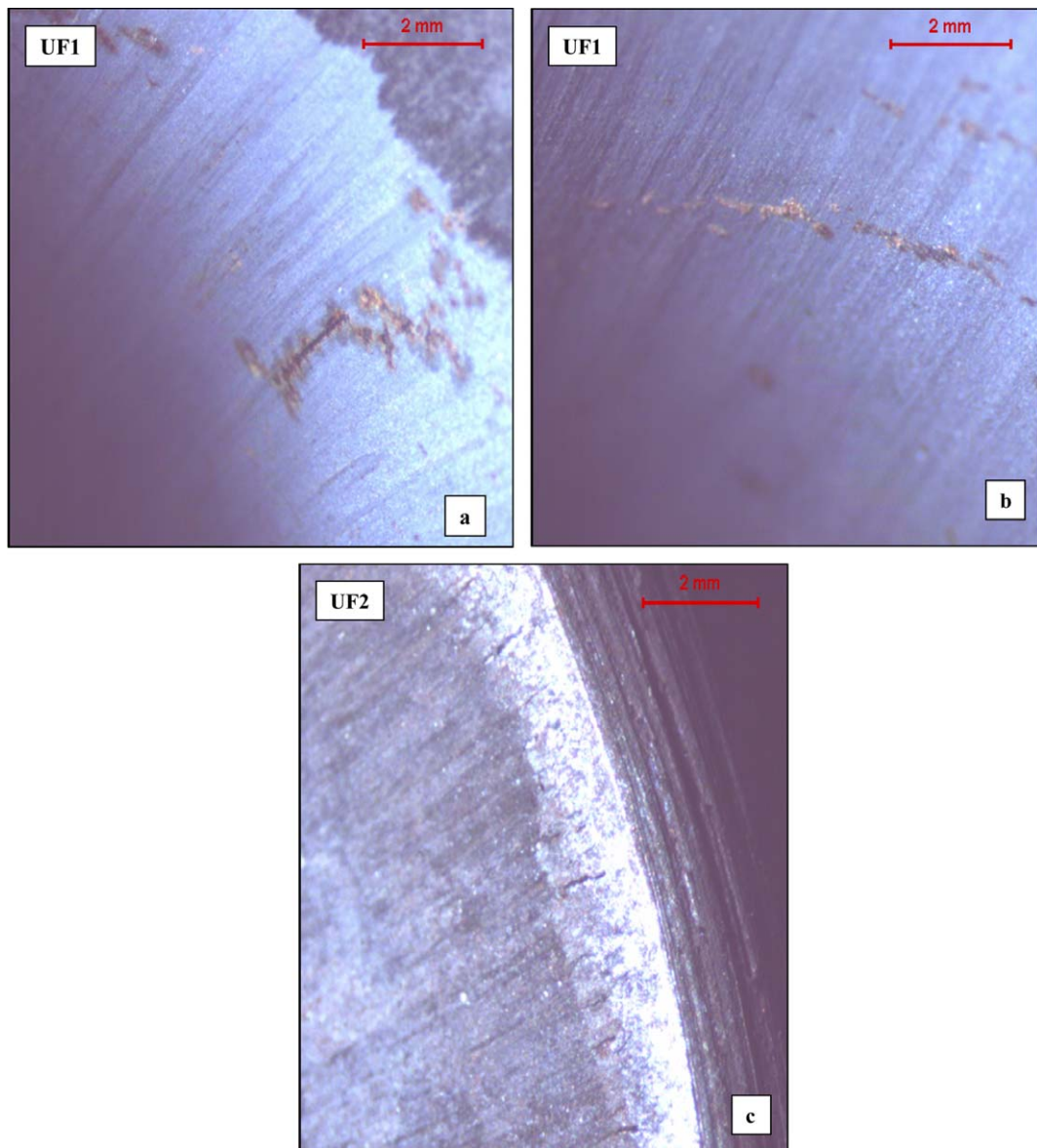


Fig. 9. Stereomicroscopic pictures of the waterside surface of the virgin tubes showing fine cracks and elongated inclusions along the rolling direction.

tial grouping of ferrite and pearlite in alternate bands aligned in the rolling direction during the sheet/plate hot-rolling operation. It is reported in the literature [3] that development of ferrite–pearlite banding is mainly due to segregation of alloying elements, principally manganese, during solidification of the ingot from which the product was rolled. The dendritic structure (ferrite dendrites and pearlite in the interdendritic areas) formed because of segregation gets rolled in to form the banded structure. Large segregation coefficients during solidification, low diffusion coefficients, large shifts in the  $A_3$  temperature and slow cooling from the austenitizing temperature are reported to favor formation of ferrite–pearlite bands. It has also been mentioned that although banding does not have a marked effect on mechanical properties, such as UTS and yield point in any direction, the reduction of area may be reduced considerably in the transverse direction (direction normal to the plane of the bands). Further, the iron oxide/manganese sulfide elongated inclusions are also found to be



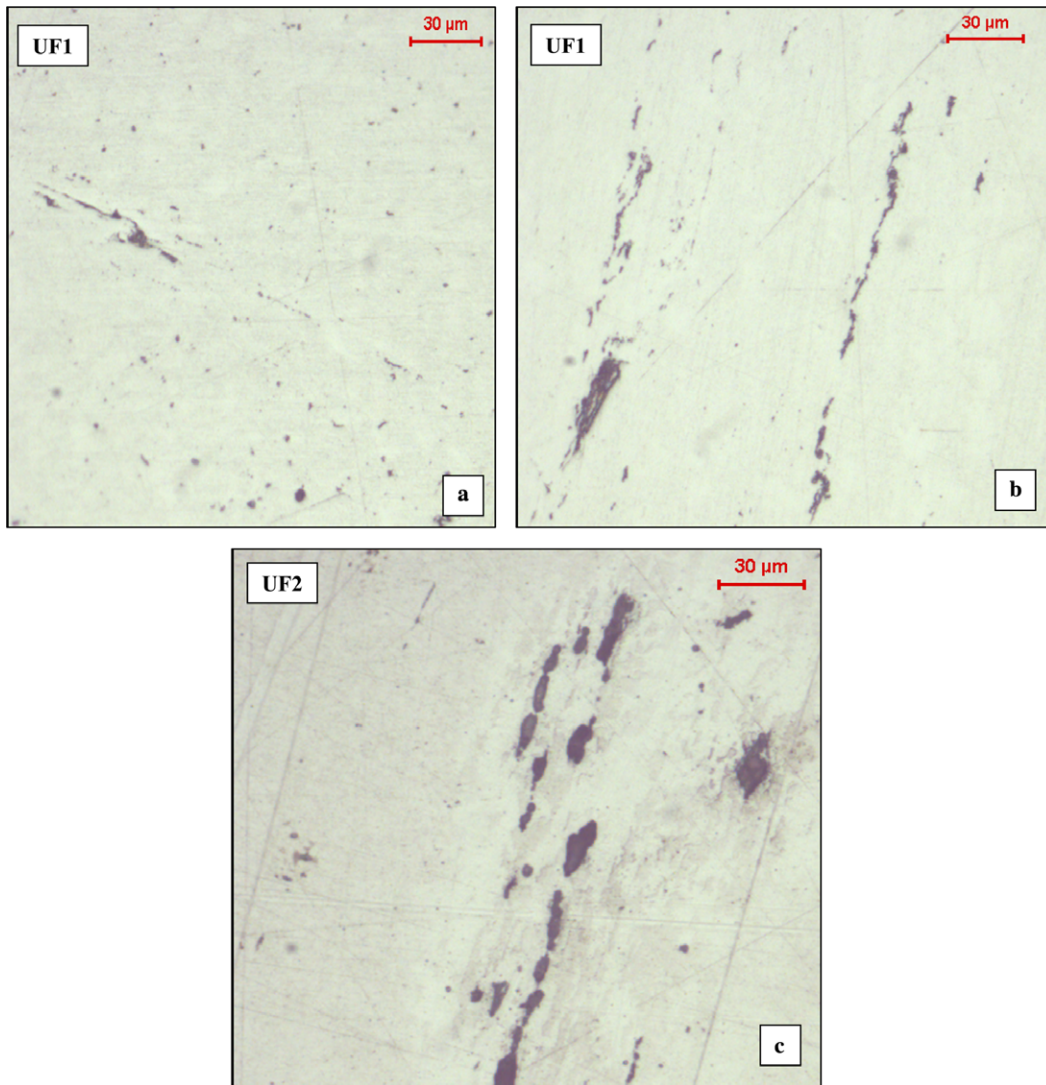


Fig. 10. Microscopic pictures in unetched condition of the virgin tube samples showing large volume fraction of sulfide type inclusions elongated along the rolling direction and interconnection of inclusions in the longitudinal direction through fine cracks.

preferentially located in the ferrite bands. These elongated inclusions located in the bands can form a lamination and further decrease the ductility in the transverse direction. The fact that all the samples failed the drift expansion test, reflects on the poor ductility of the evaporator tubes in the through thickness direction.

#### 4.1.3. State of stress in the bent evaporator tubes welded with wear plate

The absence of a stress relieving operation, both after the cold bending operation as well as after the welding of the wear plate to the bend tube is likely to result in significant residual stresses in the tubes, especially at the bend. Further, since the leg length of the weld of the wear plate to the tube is long (24 mm) due to the thickness of the wear plate and because of the long fusion zone (~116 mm) parallel to the rolling direction at both sides of the bend, the welds are likely to subject the base evaporator tube at the bend to high shrinkage stresses through the thickness of the tube. Because the fusion zone of the weld is on either sides of the tube bend, the welds are highly restrained, further increasing the stress concentration over the entire bend portion. The high values of micro- and macro-hardness (200–240 HV) at the fireside, waterside and cross-sectional surfaces at the bend region are a result of high stresses in this region. Significantly, at the fireside surface, the

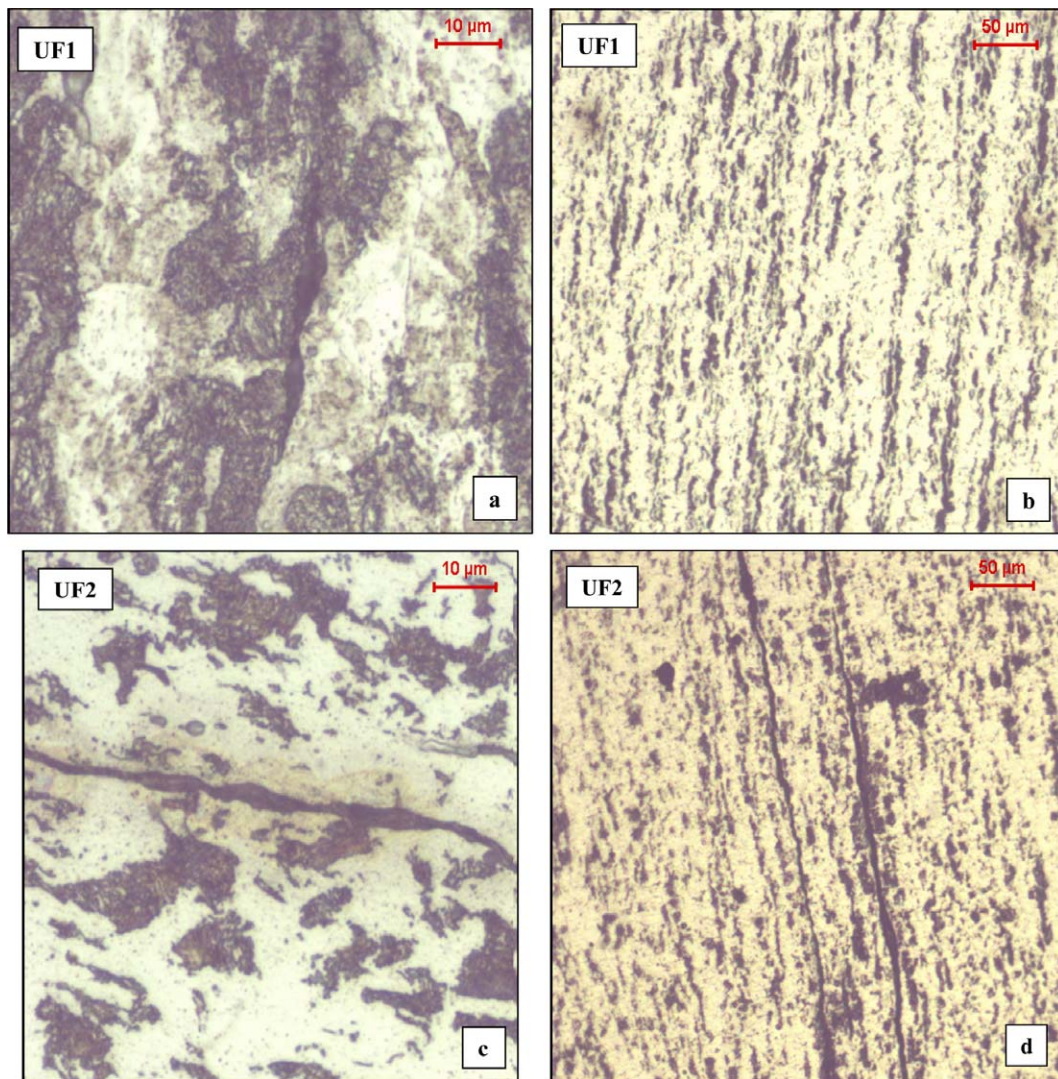


Fig. 11. Micrographs (at different magnification) in etched condition of samples cut from different locations from virgin tubes. (a) Microstructure at high magnification showing the location of elongated inclusions lying within the ferrite matrix; (b) microstructure showing a banded ferrite and pearlite structure (c) micrograph showing long elongated inclusions lying within the ferrite band and (d) microstructure showing banded ferrite and pearlite and decohesion at the boundary of the inclusion leading to cracking.

stress concentration is especially higher as observed by the very large hardness. The presence of shrinkage stresses across the thickness of the evaporator tube is also confirmed by the unexpected presence of large compressive residual stresses at the fireside surface of the outer bend of all samples.

#### 4.1.4. Pre-existing fine cracks (Lamellar tearing)

Several pre-existing fine cracks along the rolling direction are seen in the stereo-micrographs and scanning electron micrographs of the raw tube samples (both at the horizontal section and in the bend). These micro-cracks are found in the entire material. The micrographs also clearly show that the cracks are transgranular and follow the line of the inclusion stringers. The nature and features of the pre-existing cracks observed in the virgin evaporator tubes by optical and scanning electron microscopy is strongly suggestive of lamellar tearing.

In lamellar tearing, decohesion with the matrix occurs at the planar inclusions, and these decohesions are joined by short, fine cracks. Sometimes, the tear may also be initiated at groups of shorter and even angular inclusions. The cracks follow the line of the inclusion stringers and therefore show a stepped appearance.



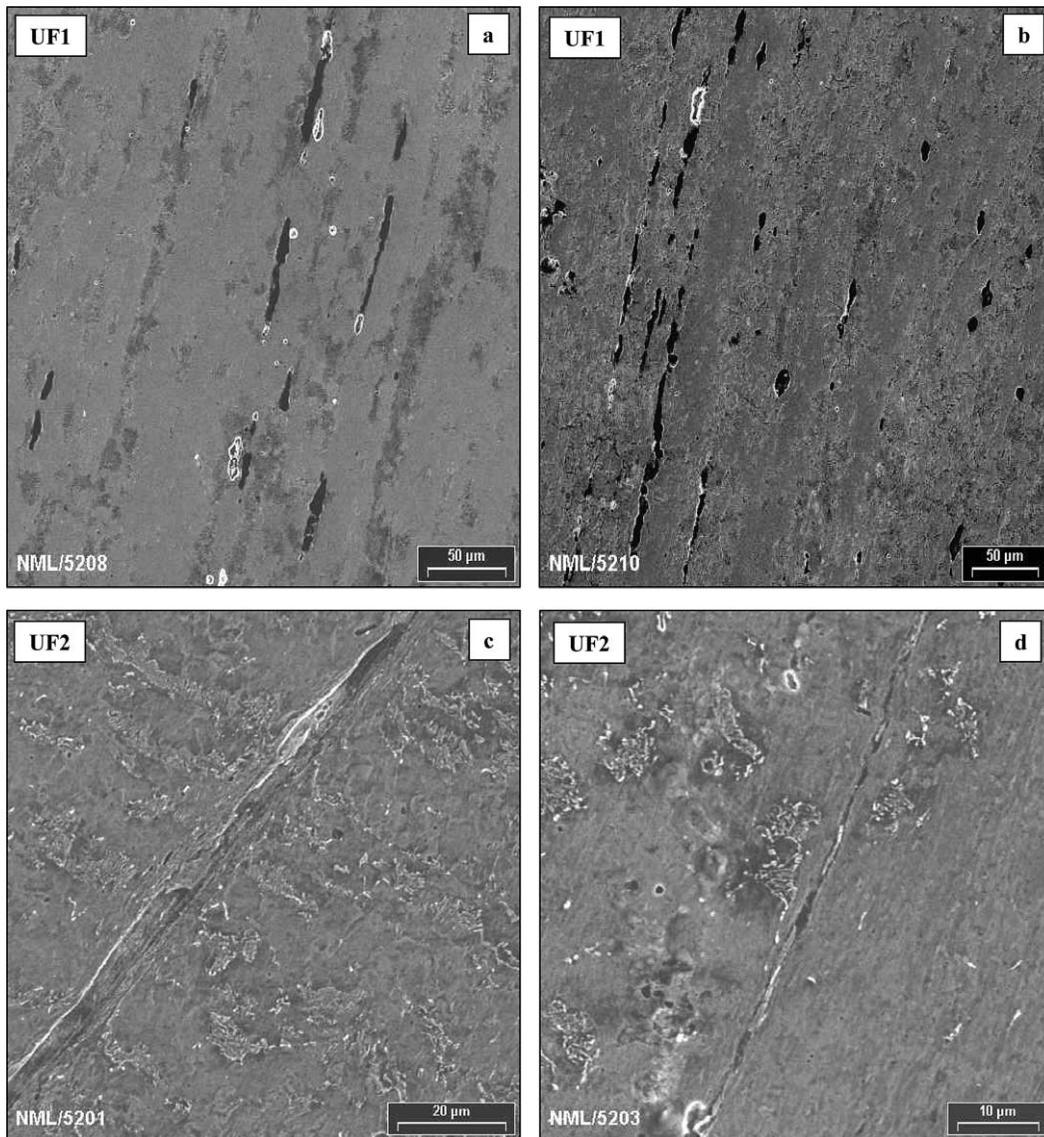


Fig. 12. Secondary electron images of polished samples from virgin tubes. (a) SEM micrograph shows elongated inclusions with two different contrasts, light gray and dark; the light gray inclusions were found to be MnS and the dark streaks were found to be iron oxide scales; (b) micrograph showing the dark iron oxide scales encapsulating the MnS stringers in some cases; (c) micrograph showing fine longitudinal cracks covered with iron oxide and (d) fine micro-cracks connecting the inclusions are evident in the SEM image.

Lamellar tears generally develop in a plane parallel to the rolling plane when high tensile stresses are applied to the plate in the short transverse direction. Lamellar tearing is more frequent in welding. It is reported that lamellar tearing takes place most commonly in the parent plate under butt welds (especially T butt joints), especially when the leg length of the weld is greater than 20 mm. It is also reported that lamellar tearing always lies within the base metal, generally outside the heat affected zone and parallel to the weld fusion boundary [5]. Susceptibility to lamellar tearing is determined essentially by the concentration of elongated inclusions oriented parallel to the surface of the plate and the consequent reduction in the short transverse reduction in area (STRA).

In the present case, the conditions, i.e., high shrinkage stresses acting in the short direction of the plate because of the long fusion zone and leg length of weld on either sides of the bend, favorable weld orientation

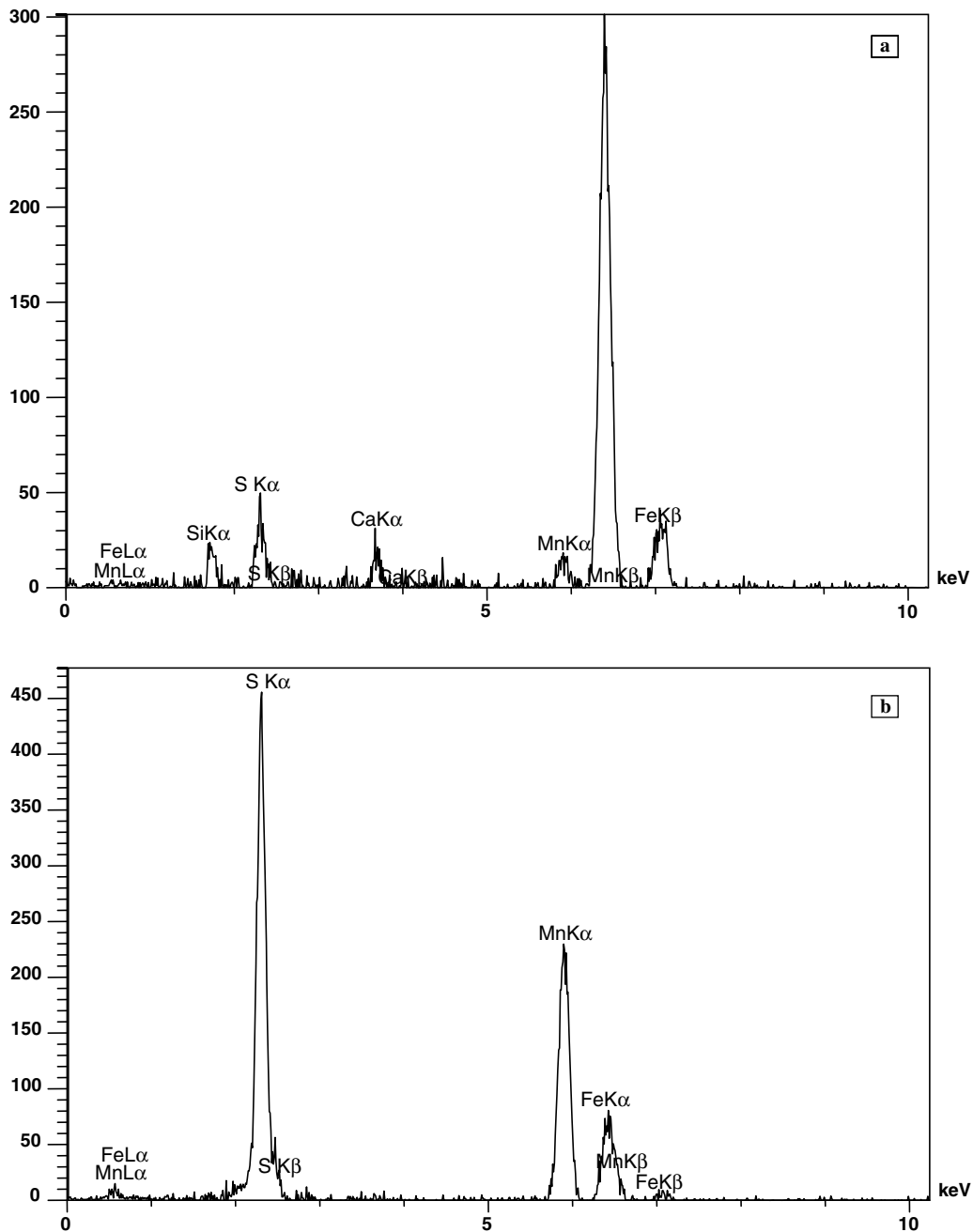


Fig. 13. (a) EDS analysis of the dark elongated inclusions seen in the bright field image confirming that these are iron oxide scales and (b) EDS analysis of the inclusions seen in light gray contrast in the bright field image revealing mainly MnS.

(fusion boundary parallel to the plane of banding and inclusions) and materials susceptibility (poor STRA values) appear to be tailor-made for lamellar cracking to occur.

#### 4.2. Defects in the failed evaporator tubes and nature of failure

Similar to the virgin tubes, the failed samples also show a large volume fraction of inclusions (mainly iron oxide and some manganese sulfide) elongated along the rolling direction, banding of ferrite and pearlite,



preferential location of the streaks/stringers of inclusions in the ferrite bands, high stress concentrations (high hardness and compressive residual stresses) in the bend especially at the fireside surface and fine micro-cracks along the rolling direction (parallel to the weld fusion boundary). All these features are characteristic of lamellar tearing observed for the virgin tubes at the bends and described in the earlier section. However, additionally, the most distinct feature of almost all the failed samples was the presence of visible long longitudinal cracks along the rolling direction at the fireside surface of the inner bend of the tube and prominently at the center of the bend. It is clear that these visible cracks have led to the ultimate rupture of the evaporator tube. These cracks appear stepped with treads parallel to the rolling plane. Fine longitudinal cracks were also observed at the waterside surface of the inner bend especially under a stereomicroscope. However, these cracks on the waterside region are not very prominent and wide as that seen at the fireside surface. It appears that the cracks initiated at the fireside surface and propagated through the thickness of the tube. It is also observed from micro-hardness measurements that the stress concentration is much higher at the fireside surface. Another unique aspect observed in the failed bend tubes was that in addition to the deep longitudinal cracks there were several micro-cracks in the transverse direction. These cracks were visible only under a microscope in an etched condition.

## 5. Conclusions

It can be concluded that the failure of the evaporator tubes at the tube bends have been initiated by lamellar tearing because of inherent defects in the material (segregation leading to banded structure), improper processing of material (rolling in of iron oxide scales with high aspect ratios as inclusions), improper design of welding (high transverse shrinkage stresses over the entire bend portion of the tube because of long fusion zone on either side of the bend and leg length of weld) and the absence of a stress relieving treatment after the cold-bending and welding operations.

Pre-existing fine (micro) longitudinal cracks in the rolling direction (parallel to the weld seam) existed in the welded evaporator tube bends because of lamellar tearing introduced by inherent material defects and shrinkage stresses during the welding. These fine cracks have subsequently opened up during the test run of the boiler when the total strain in the region increased because of steam pressure resulting in catastrophic failure of the tubes.

## References

- [1] Whiteley JH. J. Iron Steel Inst. 1948;160:365–9.
- [2] Beraha E. J. Iron Steel Inst. 1964;202:696–701.
- [3] Samuels LE. Light Microscopy of Carbon Steels. Materials Park, OH 44703-0002: ASM International; 1999.
- [4] Website <http://www.key-to-steel.com>.
- [5] Website <http://www.welding-advisors.com>.